Band alignment and barrier height considerations for the quantum-confined Stark effect

R. Y.-F. Yip,[a] P. Desjardins,[b] L. Isnard, A. Aït-Ouali, A. Bensaada, H. Marchand,[c]
J. L. Brebner, J. F. Currie, and R. A. Masut
Groupe de Recherche en Physique et Technologie des Couches Minces (GCM), Département de Génie Physique, Ecole Polytechnique de Montréal, et Département de physique, Université de Montréal, C.P. 6079, succ. ''Centre-Ville,'' Montréal, QC Canada H3C 3A7

(Received 20 August 1997; accepted 4 November 1997)

Strained-layer multiple quantum wells InAsP/InP and InAsP/InGaP optical modulators based on the quantum-confined Stark effect have been fabricated from layers grown by metalorganic vapor phase epitaxy on InP(001). The device layers have been characterized by complementary high resolution x-ray diffraction, transmission electron microscopy, optical absorption and photoluminescence analyses. The structural properties of the layers were deduced from the above data and an accurate determination of the band alignment of the heterostructures was made by performing multiple transition fits to the optical absorption spectra using the Marzin–Bastard envelope function model for strained-layer superlattices. The electric field-dependent redshift of the fundamental electron-heavy hole transition was measured by a photocurrent method and found to be enhanced for structures with lower valence band barrier heights. This observation leads directly to the conclusion that the overall performance of high speed, low drive voltage optical modulators may be improved by engineering the band alignment of the multiple quantum well stack towards structures with disproportionately large conduction band offsets. An optimization of the band alignment will permit more efficient optical modulation by reducing the drive field required to operate the device, which, in turn, can have direct effects upon the drive voltage, device capacitance, attenuation coefficient, and optical coupling and propagation losses.
[S0734-2101(98)04102-5]

I. INTRODUCTION

Extensive engineering of band line-ups is becoming a practical method for boosting device performance because of the expanding range of heterojunctions made available to device and system designers by advances in the growth and characterization of IV-IV, III-V and II-VI semiconductor alloys. The most visible application of this is the engineering of heterojunction band line-ups for electronic transport devices.[1] In this article, we show that the design of the multiple quantum well stack (MQWS) for the quantum-confined Stark effect[2] (QCSE) devices[3–6] is also a model problem in band line-up engineering.

Experimental data obtained for QCSE optical modulators fabricated from strained InAsP/InP and strain-compensated InAsP/InGaP MQWSs grown on InP(001) indicate that the drive field required to operate the devices can decrease significantly for decreasing valence band (VB) discontinuities.[7,8] Therefore, since premature delocalization[9–11] of the conduction band (CB) eigenstate is usually the main reason for loss of oscillator strength with increasing field, device performance may be improved by using MQWSs with asymmetrically large CB offsets to simultaneously balance the wave function leakage and reduce the drive field.[12] This is a consequence of the large difference between the CB and VB effective masses in III-V semiconductors. It should be possible to optimize the performance of QCSE devices by using an asymmetric band line-up to compensate the effective mass asymmetry.

II. EXPERIMENT

Strained-layer MQWSs were prepared by low-pressure metalorganic vapor phase epitaxy using trimethyl-indium, trimethyl-gallium, tertiarybutyl-arsine and phosphine precursors. Growth on S-doped ($\sim 2\times10^{18}$ cm^{-3}) InP (001) substrates was performed using Pd-purified H_2 as a carrier gas and substrate temperatures of 600 °C for InAsP/InP and 620 °C for InAsP/InGaP. A nominal 100 nm buffer layer of undoped InP was grown, followed by the MQWS and then a 300–500 nm Zn-doped cap layer for the *p* contact. The structural characteristics of the samples determined from high resolution x-ray diffraction (XRD) and transmission electron microscopy (TEM) analyses are summarized in Table I. Optical absorption spectra at 8 K and at room temperature were measured for the as-grown epitaxial layers using a free-flow, He-circulating cryostat, BOMEM DA3 Fourier transform interferometric spectrometer with a quartz halogen source and Ge photodetector. The band offsets, barrier heights and n=1 quantized levels at the CB and VB have been determined using the method described by Marzin *et al.*[13–15] to perform multiple transition fits of the positions of optical absorption peaks with the structural data and state

[a]Electronic mail: ryip@email.phys.polymtl.ca
[b]Present address: Coordinated Science Laboratory, University of Illinois at Urbana-Champaign, IL 61801.
[c]Present address: Department of Electrical and Computer Engineering, University of California at Santa Barbara, CA 93106-9560.

TABLE I. Sample listing. The layer thicknesses and compositions are determined from a combination of high-resolution x-ray diffraction, transmission electron microscopy and optical absorption measurements. The barrier heights and E_1 levels are obtained by fitting quantum well transitions calculated using the Marzin–Bastard model for strained-layer superlattices to transitions measured by optical absorption at 8 and 300 K. The terms e1, hh1, and lh1 refer, respectively, to the $n=1$ levels in the conduction, heavy hole and light hole bands. The effective masses in the direction of the quantum confinement potential are linear interpolations between InAs and InP, given in units of the free electron mass, m_0.

Sample	Structure	Barrier heights			E_1 levels			Effective masses		
		e1	hh1	lh1	e1	hh1	lh1	e1	hh1	lh1
		(meV)	(meV)	(meV)	(meV)	(meV)	(meV)	(m_0)	(m_0)	(m_0)
mod05	$25\times$(9.8 nm $InAs_{0.100}P_{0.900}$/9.8 nm InP)	73	25	5	20	3.5	3.8	0.0734	0.626	0.111
mod06	$25\times$(10.3 nm $InAs_{0.156}P_{0.844}$/10.3 nm InP)	113	39	10	24	3.7	6.1	0.0703	0.613	0.095
gp24	$20\times$(8.4 nm $InAs_{0.26}P_{0.74}$/9.6 nm $In_{0.88}Ga_{0.12}P$)	210	120	5	38	6.5	3.8	0.065	0.59	0.095

of strain in the multilayers measured by XRD and TEM as inputs in an envelope function model for strained-layer superlattices. Room temperature measurements of the electric field-induced Stark shift of the quantum well optical transitions were performed by detecting the photocurrent response of the diodes as a function of reverse bias voltage using a tungsten lamp source, 0.3 m scanning monochromator and lock-in amplifier. Details on growth and characterization of these MQWSs and the fabrication and characterization of the photodiodes are presented in Refs. 7, 8 and 16.

III. RESULTS AND DISCUSSION

The field-induced redshift, ΔE_1, of the fundamental energy level in a quantum well is given approximately by[7]

$$\Delta E_1 \sim F^2 L^2 / E_1, \tag{1}$$

where F is the magnitude of the electric field, L is the well width and E_1 is the energy of the level measured with respect to the bottom of the quantum well at flatband. The effective mass of the VB is much larger than that of the CB. Therefore, E_1 is correspondingly smaller in the VB and the VB component makes the dominant contribution to the redshift of the optical transition. Through its influence on E_1 in the VB, the VB barrier height can significantly affect the overall redshift per unit applied field. The redshift of the $n=1$ electron-heavy hole transition for each sample is plotted as a function of electric field in Fig. 1. The redshift response for a strain-balanced $InAs_{0.53}P_{0.47}/In_{0.84}Ga_{0.16}P$ MQWS[17] and for an $In_{0.53}Ga_{0.47}As/In_{0.52}Al_{0.48}As$ MQWS[18] lattice matched to InP, both operating near 1.55 μm, have been included for comparison. The curves (a), (b), (c), (d), and (e) correspond to MQWSs with $L\sim 10$ nm, similar CB and VB effective masses and respective VB barrier heights of 25, 39, 52, 200 (estimated), and 250 meV (estimated). This shows that non-trivial drive field reductions may be achieved by using small VB discontinuities.

In response to an electric field, the electron and hole eigenstates follow the contours of the linear energy gradient in opposing directions so that a large redshift necessarily induces a strong polarization of the eigenstates with the corresponding reduction in the oscillator strength of the absorption resonance. This also means that heterostructures exhibiting enhanced resistance to field quenching of the resonance tend to display correspondingly less prominent redshifts per unit field. Therefore, band structure designs must target an optimal compromise according to the specific requirements of the application. The performance of three MQWSs is compared using two figures of merit (Table II). The modulation depth per unit drive field, $\Delta\alpha/F$, is commonly used to compare the performance of optical modulators. $\Delta\alpha/F^2$ is inversely proportional to the average power per unit bandwidth required to operate the modulator and is important for high frequency applications.[19] In compiling the data for Table II, we restricted our attention to the region of low on-state loss below the band edge for which $\alpha_0 < \sim 500$ cm^{-1}. The term t is the total thickness of quantum well material. Despite large variations in the CB and VB discontinuities (V_e and V_h), modulation depth ($\Delta\alpha$), and drive field (F), $\Delta\alpha/F$ is remarkably similar across the set of samples. This is consistent with the principle of balance between modulation depth and drive field. The values for $\Delta\alpha/F^2$ show that balanced low VB barrier designs can

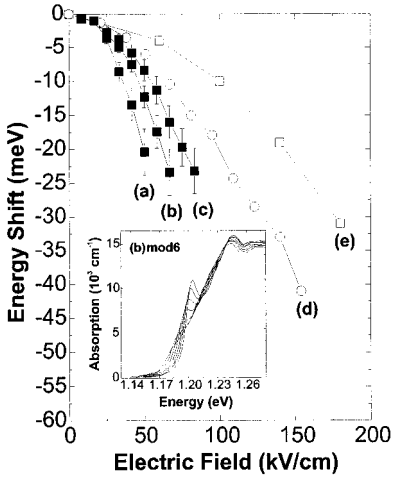

FIG. 1. Energy redshift of the $n=1$ electron-heavy hole transition as a function of electric field. The curves for (a) $25\times$(9.8 nm $InAs_{0.100}P_{0.900}$/9.8 nm InP) (mod05), (b) $25\times$(10.3 nm $InAs_{0.156}P_{0.844}$/10.3 nm InP) (mod06), (c) $25\times$(9.8 nm $InAs_{0.264}P_{0.736}$/9.8 nm InP) (mod04) are obtained from photocurrent spectra. Curve (d) is data for a $40\times$(10.5 nm $In_{0.53}Ga_{0.47}As$/6.8 nm $In_{0.52}Al_{0.48}As$—lattice matched to InP) MQWS from Ref. 18 and curve (e) is data for a $21\times$(10.0 nm $InAs_{0.53}P_{0.47}$/14.0 nm $In_{0.84}Ga_{0.16}P$) strain-balanced MQWS from Ref. 17, operating at 1.55 μm. The inset figure shows the photocurrent curves (electric field response of the optical absorption) for sample (b) mod06.

TABLE II. Comparison of the multi-quantum well stacks studied in this article using two common figures of merit for optical modulators. The samples are listed from top down in order of increasing total barrier height. $\Delta\alpha$ is the change in absorption coefficient available at an applied electric field, F. The $\Delta\alpha$ values are measured in the region of low on-state loss (low energy tail of the exciton resonance) for which $\alpha_0 < 500\ \mathrm{cm}^{-1}$. The term t is the total thickness of quantum well material available for electroabsorption. This demonstrates the trade-off between modulation depth and drive field as a function of barrier height.

Sample	ΔE_C (meV)	ΔE_{Vhh} (meV)	$\Delta\alpha$ (cm^{-1})	F (kV/cm)	$t(\mu\mathrm{m})$	$\Delta\alpha/F$ (kV^{-1})	$\Delta\alpha/F^2$ ($\mathrm{cm/kV}^2$)
mod5d	73	25	1500	25 at 1.5 V	0.245	60	2.40
mod6b	113	39	2900	40 at 2.5 V	0.258	73	1.81
gp24b	210	120	6200	88 at 4.0 V	0.168	70	0.80

significantly outperform high VB barrier designs in high frequency applications. It is evident that the performance of high barrier MQWSs such as lattice-matched $In_{0.53}Ga_{0.47}As/In_{0.52}Al_{0.48}As$ or strain-compensated $InAs_{0.53}P_{0.47}/In_{0.84}Ga_{0.16}P$ on InP for high data rate telecommunications is hampered by the high VB barriers which require large drive fields to induce significant redshifts. Elevated drive fields require that the device active regions (i.e. junction widths) be significantly thinner than the characteristic dimension of the optical mode (typically $\lambda/n \sim 0.45$ μm, where n is the refractive index of the material). This has four notable disadvantages:

(1) A thin active modulator core is a poorly proportioned waveguide cavity for the optical mode, leading to greater propagation losses in the modulator section. It increases the mismatch between the dimensions of the modulator waveguide and both the core of the optical fiber waveguide and active width of the laser so that in- and out-coupling losses are greater.[19,20]

(2) High barriers make the removal of photocharge from the quantum wells less efficient. Charge pileup in the wells can saturate the QCSE modulation and limit the incident optical intensities that may be tolerated.[21–23]

(3) A thin junction increases the device capacitance, which increases the power required to drive the load and also decreases the frequency response bandwidth of the load.

(4) A thin junction restricts the volume of active material available for electroabsorption. Therefore, in direct comparisons of $\Delta\alpha$ between high and low barrier MQWSs, the larger values available in high barrier structures are somewhat misleading.

For high frequency applications, our data (Table II) indicate that low VB barrier samples are a better choice despite the penalty in modulation depth ($\Delta\alpha$) because they allow the designer to use the advantages of a low drive field MQWS to address any combination of the issues (1)–(4) plus the drive voltage. This allows for greater flexibility in the design of the optical modulator, the drive electronics and the coupling of modulator to the laser and optical fiber.

In Refs. 7 and 12, calculations showed that useful reductions in the drive field may be achieved with VB barrier heights lower than $\sim$ 60–100 meV. Next, to extract the full potential of the low VB barrier, it is important that the CB barrier be sufficiently high so that premature delocalization of the CB wave function does not dominate the overall behavior. The calculations of Refs. 8 and 12 showed that a CB barrier 3–9 times higher than the VB barrier would be required for an optimal structure with balanced wave function leakage when the electron and hole effective masses are, respectively, 0.055 m_0 and 0.5 m_0 (m_0 is the free electron mass).[24]

Fig. 2 illustrates two promising candidates for the target band structure with large conduction band offset and quantum well band gap suitable for operation at 1.3 and 1.55 μm. First, consider the strained InAsP/InGaAsP system on InP(001) shown on the left. The strained line-up of $InAs_xP_{1-x}/InP$ for $\{0 < x \leqslant 1\}$ corresponds to $V_e/V_h \sim 3-4$. The lattice-matched $In_yGa_{1-y}As_zP_{1-z}/InP$ line-up corresponds to $V_e/V_h \sim 0.5-1.0$. Therefore, the band line-up of InAsP/InGaAsP grown on InP for strained wells and lattice-matched barriers should yield $V_e/V_h \geqslant \sim 3-4$. A well made from InAsP in the 0.8–0.95 eV range and a barrier made from InGaAsP nearly lattice matched to InP in the 0.90–1.15 eV range should give a VB barrier in the target 25–60 meV range with the desired band offset asymmetry. However, operation at 0.8 and 0.95 eV would require $\sim$ 10 nm wide wells with, respectively, $\sim$1.8% and $\sim$1.4% compressive strains. So for a thick MQWS, the use of tensile strained

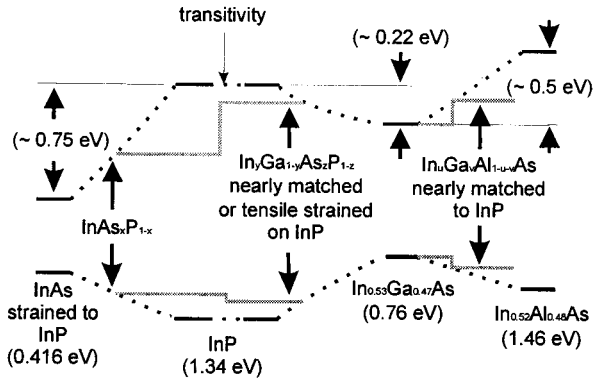

FIG. 2. Two strategies for obtaining heterojunctions with large conduction band offsets, small valence band discontinuities in the 25–60 meV range and a fundamental optical transition energy near 0.8 or 0.95 eV. The band alignments shown for the $In_{0.53}Ga_{0.47}As/InP$ and $In_{0.53}Ga_{0.47}As/In_{0.52}Al_{0.48}As$ heterojunctions correspond to widely accepted values (see Ref. 25). The band alignment shown for the strained $InAs_xP_{1-x}/InP(001)$ heterojunction corresponds to the experimentally determined values in Ref. 15, and agrees well with the model predictions of Ref. 26.

barriers is likely necessary to compensate the large compressive strain in the InAsP wells. Next, we may also consider the nearly lattice matched InGaAs/InGaAlAs system on InP(001) shown on the right. The $In_{0.53}Ga_{0.47}As/In_{0.52}Al_{0.48}As$ system lattice matched to InP is suitable for operation at 0.8 eV and reported to have a favorable band line-up with $V_e/V_h \sim 2.5$. But, the barrier heights are too high, especially the $\sim$200 meV VB barrier. Ga and Al may be substituted for each other to change the band gap energy of the barrier without inducing large strains. So, the line-up of $In_{0.53}Al_xGa_{0.47-x}As/In_{0.52}Al_yGa_{0.48-y}As$ lattice matched to InP is expected to retain a nearly constant V_e/V_h ratio for $\{0 \leqslant x \leqslant 0.47,\ 0 \leqslant y \leqslant 0.48;\ x < y\}$. The band alignment depends strongly on the state of strain at the heterojunction interface. In both cases, extensive strain tuning of the alignment is possible and the goal is to find the combinations of wells and barriers that give the desired band line-up with net strains that are small enough to permit the growth of thick MQWSs.

IV. CONCLUSIONS

We propose the following two principles for designing the band structure of the MQWS in QCSE devices:

(1) Balancing energy redshift enhancements versus loss of oscillator strength with an appropriate choice of the VB barrier height to suit application-dependent drive field versus optical modulation depth requirements.

(2) Balancing the wave function leakage at the CB and VB with an asymmetric band alignment.

The asymmetric band line-up compensates the effects due to the effective mass difference between CB and VB. In many cases, and especially for high speed, low drive voltage applications, it is advantageous to pursue balanced designs incorporating relatively low VB barrier heights to enhance field sensitivity and reduce the drive field. This can improve the overall performance by permitting a lower drive voltage and/or wider diode junction with larger active volume, lower capacitance, lower propagation losses and improved laser-modulator and modulator-fiber coupling. A MQWS possessing the desired band alignment and VB barrier heights that is capable of operating in the 1.3–1.55 μm range for optical telecommunications should be achievable using a combination of strained III-V semiconductor alloys that are commonly grown onto InP(001) substrates.

ACKNOWLEDGMENTS

The authors thank Dr. Mario Beaudoin for providing the computer program used to calculate the energy levels in a strained-layer superlattice, and Gino Turcotte and Joël Bouchard for technical assistance in realizing this study. This work was supported by the Natural Sciences and Engineering Research Council (NSERC) of Canada and the Fonds pour la Formation de Chercheurs et l'aide à la Recherche (FCAR) du Québec.

[1]F. Capasso, in *Heterojunction Band Discontinuities, Physics and Device Applications* edited by F. Capasso and G. Margaritondo (Elsevier, Amsterdam, 1987), p. 399.
[2]D. A. B. Miller, D. S. Chemla, T. C. Damen, A. C. Gossard, W. Wiegmann, T. H. Wood, and C. A. Burrus, Phys. Rev. B **32**, 1043 (1985).
[3]D. M. Adams, C. Rolland, N. Puetz, R. S. Moore, F. R. Shepherd, H. B. Kim, and S. Bradshaw, Electron. Lett. **32**, 485 (1996).
[4]M. Aoki, M. Suzuki, M. Takahashi, H. Sano, T. Ido, T. Kawano, and A. Takai, Electron. Lett. **28**, 1157 (1992).
[5]A. V. Krishnamoorthy, A. L. Lentine, K. W. Goosen, J. A. Walker, T. K. Woodward, J. E. Ford, G. F. Aplin, L. A. D'Asaro, S. P. Hui, B. Tseng, R. Leibenguth, D. Kossives, D. Dahringer, L. M. F. Chirovsky, and D. A. B. Miller, IEEE Photonics Technol. Lett. **7**, 1288 (1995).
[6]Anthony L. Lentine and David A. B. Miller, IEEE J. Quantum Electron. **29**, 655 (1993).
[7]F. Y.-F. Yip, A. Aït-Ouali, A. Bensaada, P. Desjardins, M. Beaudoin, L. Isnard, J. L. Brebner, J. F. Currie, and R. A. Masut, J. Appl. Phys. **81**, 1905 (1997).
[8]R. Y.-F. Yip, P. Desjardins, L. Isnard, A. Aït-Ouali, H. Marchand, J. L. Brebner, J. F. Currie, and R. A. Masut, J. Appl. Phys. (submitted).
[9]W. L. Bloss, J. Appl. Phys. **65**, 4789 (1989).
[10]T. Yamanaka, K. Wakita, and K. Yokoyama, Appl. Phys. Lett. **65**, 1540 (1994).
[11]T. Ikeda and H. Ishikawa, IEEE J. Quantum Electron. **32**, 284 (1996).
[12]R. Y.-F. Yip and R. A. Masut, J. Appl. Phys. **82**, 1976 (1997).
[13]J. Y. Marzin, J. M. Gérard, P. Voisin, and J. A. Brum, in *Semiconductors and Semimetals* (Academic, San Diego, 1990), Vol. 32, p. 55.
[14]G. Bastard, *Wave Mechanics Applied to Semiconductor Heterostructures* (Les Éditions de Physique, Les Ulis Cedex, France, 1988).
[15]M. Beaudoin, A. Bensaada, R. Leonelli, P. Desjardins, R. A. Masut, L. Isnard, A. Chennouf, and G. L'Espérance, Phys. Rev. B **53**, 1990 (1996).
[16]P. Desjardins, H. Marchand, L. Isnard, and R. A. Masut, J. Appl. Phys. **81**, 3501 (1997).
[17]X. B. Mei, W. G. Bi, C. W. Tu, L. J. Chou, and K. C. Hsieh, J. Vac. Sci. Technol. B **14**, 2327 (1996).
[18]S. Nojima, Y. Kawamura, K. Wakita, and O. Mikami, J. Appl. Phys. **64**, 2795 (1988).
[19]M. K. Chin, IEEE Photonics Technol. Lett. **4**, 726 (1992).
[20]O. Mitomi, I. Kotaka, K. Wakita, S. Nojima, K. Kawano, Y. Kawamura, and H. Asai, Appl. Opt. **31**, 2030 (1992).
[21]T. H. Wood, J. Z. Pastalan, C. A. Burrus, Jr., B. C. Johnson, B. I. Miller, J. L. deMiguel, U. Koren, and M. G. Young, Appl. Phys. Lett. **57**, 1081 (1990).
[22]A. M. Fox, D. A. B. Miller, G. Livescu, J. E. Cunningham, and W. Y. Jan, IEEE J. Quantum Electron. **27**, 2281 (1991).
[23]F. Devaux, S. Chelles, A. Ougazzaden, A. Mircea, and J. C. Harmand, Semicond. Sci. Technol. **10**, 887 (1995).
[24]These values correspond to InGaAsP alloys with energy band gaps in the 0.8–0.95 eV range for optical fiber telecommunications.
[25]E. T. Yu, J. O. McCaldin, and T. C. McGill, in *Solid State Physics* (Academic, San Diego, 1994), p. 33.
[26]J. Tersoff, Phys. Rev. B **30**, 4874 (1984); J. Tersoff, in *Heterojunction Band Discontinuities, Physics and Device Applications*, edited by F. Capasso and G. Margaritondo (Elsevier, Amsterdam, 1987), p. 3.